Papers

The Impact of Various Imaging Parameters on Ultrasonic Displacement and Velocity Estimates

Eric J. Chen, W. Kenneth Jenkins, *Fellow, IEEE,* and William D. O'Brien, Jr., *Fellow, IEEE*

Abstract—**The accuracy of displacement and velocity data in ultrasonic motion detection systems depends on a combination of ultrasonic imaging parameters. These include magnitude and direction of target motion, target region dimensions, scattering media, ultrasonic frequency of interrogation, digital sampling frequency, and signal type (envelope detected or RF). Because the impact of scattering media in particular has heretofore received little or no attention, we provide experimental results and computer analysis to evaluate the influence of different scattering media on the accuracy of ultrasonic displacement and velocity estimates using porcine liver, porcine muscle, and woolen sea sponge samples. Our experimental results show that for identical target dimensions and displacements, the accuracy of ultrasonic displacement and velocity estimates in porcine muscle samples are substantially higher than in porcine liver samples. Analysis of experimentally derived autocovariance curves for each tissue type indicates that the improvement in accuracy for muscle samples is not, in fact, due to differences in the speckle characteristics for each tissue type. The improvement is attributed to the presence of well-defined and resolvable image structures from muscle and the lack of such resolvable structures in porcine liver tissue. We provide a summary of the factors impacting ultrasonic displacement and velocity measurements, and discuss why and how a combination of one or more imaging parameters affects these measurements.**

I. Introduction

In many medical ultrasound imaging systems, clinical data are computed from estimates of tissue displacement and tissue velocity. These data are often interpreted by the physician en route to diagnosis. An often overlooked aspect of the process is the importance for the clinician to understand to what degree the data are reliable. Clinical diagnoses are only as good as the data on which they are based. There are a number of important factors that contribute to the accuracy of ultrasonic tissue displacement and velocity estimates, and many of these have been reported.

Chen *et al.* [1]–[3] discuss the importance of tracking targets over small distances and through a large number of positions, as opposed to tracking over large distances and through fewer positions. This result is due to the fact that ultrasonic displacement and velocity estimates deteriorate with increasing target displacements.

Manuscript received March 4, 1993; revised October 3, 1993. This work was supported by the National Institutes of Health, National Cancer Institute under Grant CA 09067 and by the National Live Stock and Meat Board.

The authors are with the Department of Electrical and Computer Engineering, University of Illinois, Urbana, IL 61801 USA.

IEEE Log Number 9400142.

Ramamurthy and Trahey [4] have reported an improved accuracy for measurements taken in the axial direction over the lateral direction. They also note a substantial improvement in both directions when using RF data instead of envelope-detected signals. Wagner *et al.* [5] have provided theoretical predictions on the statistics of speckle, and their results have been experimentally verified [4], [5].

Foster *et al.* [6] found that scatters moving at different velocities in the target region or range cell limit the accuracy of velocity estimates. Chen *et al.* [1]–[3] and Ramamurthy and Trahey [4] have reported that ultrasonic displacement estimates deteriorate with decreasing region of interest (ROI) dimensions in two-dimensional tissue tracking, and Foster *et al.* [6] reported similar results for one-dimensional blood flow measurements. Here, ROI dimensions refer to the dimensions of a region of interest selected from an image, not the physical size of the object being imaged.

Parilla *et al.* [7] compared the performance of $L1$ norm, $L2$ norm, and correlation techniques in ultrasonic range measurements in air. They report that for low signal-to-noise environments, correlation techniques (locating the time shift producing the highest correlation between the transmitted and received echoes) provide more accurate range estimates than $L1$ norm or $L2$ norm techniques. In their study, $L1$ and $L2$ norm techniques consisted of locating the time shift producing the smallest absolute difference and squared difference between the transmitted and received echoes. Their simulation results also suggest that by sampling four–five times the fundamental signal frequency noise becomes the limiting factor with regard to accuracy. In low signal-to-noise ratio environments, Ferrara [8] and Ramamurthy and Trahey [4] have reported that correlation techniques perform similarly to Doppler-based techniques.

Chen *et al.* [1]–[3], Ramamurthy and Trahey [4], and Foster *et al.* [6] suggest that accuracy will improve with increasing ultrasonic frequency of interrogation. This result stems from the increase in spatial resolution which is traded off against a decrease in depth of penetration.

The impact of scattering media on ultrasonic displacement and velocity measurements has not received significant attention. To evaluate the effect of different scattering media on ultrasonic displacement and velocity estimates, we have assessed the accuracy of ultrasonic displacement estimates of ROI's in porcine liver, porcine muscle, and woolen sea sponge samples. Our results show that ultrasonic displacement estimates were

0885–3010/94$04.00 © 1994 IEEE

best in muscle samples and worst in liver samples. This result is attributed to the heterogeneous composition of muscle which contains thousands of well-defined fibers, in various orientations, surrounded by connective tissue, and the more homogeneous composition of liver which is predominantly composed of more structurally generic parenchymal cells [10]–[14].

II. Ultrasonic Motion Detection Method

A. Ultrasonic Time Domain Correlation Speckle-Tracking Technique

The cross-correlation speckle-tracking technique is based on the normalized correlation coefficient and can be used to detect motion [1]–[4]. To illustrate the technique, we consider a number of ultrasonic images, taken temporally in series, from a moving target. A user-defined region of interest (ROI) is selected or windowed out from the first image [Fig. 1(a)–(d)]. The windowed region of the first image is spatially shifted and correlated with identically sized regions of the second image. A rectangular search area centered on the starting position of the ROI, and extending out by 1.0 cm in each dimension, is automatically selected, regardless of the ROI dimensions. At each spatial shift, the normalized correlation coefficient (1) is computed between the ROI from the first image and the "range cell" or "target region" from the second image, giving

$$\rho_{xy}(k,l) = \frac{\sum_{i=0}^{M}\sum_{j=0}^{N}(x_{i,j}-\overline{x})(y_{i+k,j+1}-\overline{y})}{\sqrt{\sum_{i=0}^{M}\sum_{j=0}^{N}(x_{i,j}-\overline{x})^2\sum_{i=0}^{M}\sum_{j=0}^{N}(y_{i+k,j+1}-\overline{y})^2}}. \tag{1}$$

The normalized correlation coefficient (1) has been implemented in two-dimensional search algorithms [1]–[4]. Here, $x(i,j)$ represents the amplitude inside the first image at the pixel coordinates (i,j), and $y(i+k,j+l)$ represents the amplitude inside the second image at the pixel coordinates $(i+k,j+l)$. This is further illustrated in Fig. 1(e).

Assuming the object being imaged covers most or all of the field of view of the image, the physical size (dimensions) of the object will typically be much larger than the dimensions of any ROI selected from an image. In this paper, the terms "ROI dimensions" and "target region dimensions" refer to the dimensions of regions of interest selected from images. They do not refer to the physical size (dimensions) of the object being imaged.

By plotting the normalized correlation coefficients as a function of the spatial shifts, a cross-correlation function between the two images can be generated. The spatial shift corresponding to the peak correlation value can be used with the elapsed time between the initiation of ultrasonic images to determine both displacement and velocity.

B. Incremental Tracking Strategy

We now consider the problem of tracking the position of a moving target in one or two dimensions, given a number of reflected echoes of the target received at different times. If the echoes are received at roughly equally spaced temporal intervals, and if the target is moving with constant velocity, then the movement of the ROI between the first and last echoes can be estimated in two ways. The direct approach is to window out the portion of the first echo which corresponds to the target, and then apply a cross-correlation search to the first and last echoes [1], [2]. This is shown schematically in Fig. 2(a) by a pair of square pulses. Using a cross-correlation

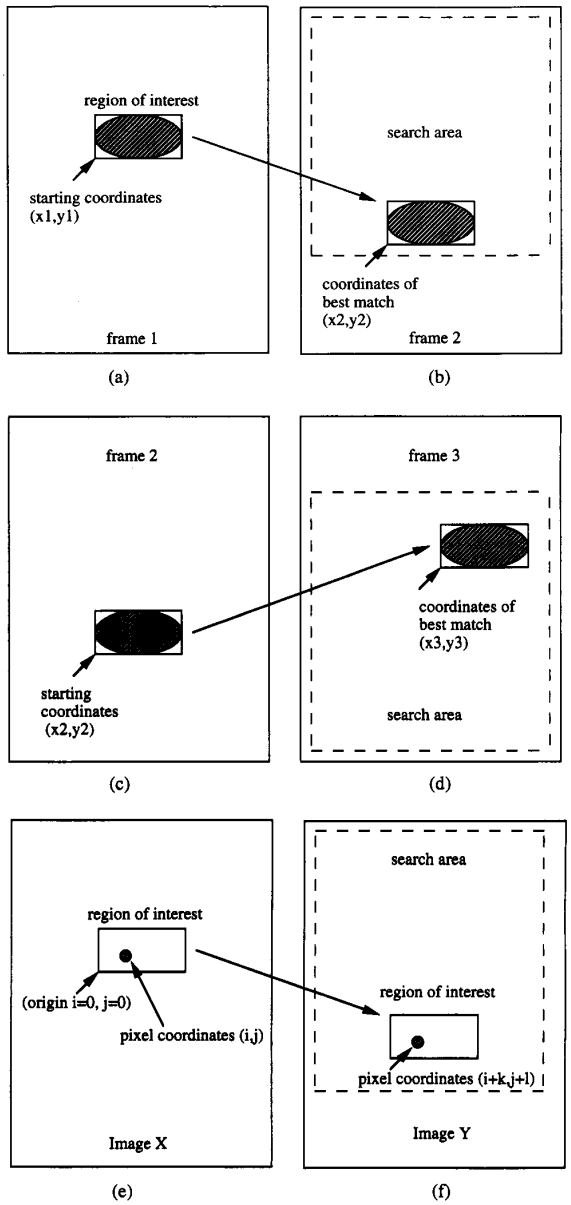

Fig. 1. Two-step procedure for frame-to-frame correlation speckle tracking. (a) A user-defined region of interest (ROI) with coordinates $(x1, y1)$ is selected from the first frame. (b) The position of the best correlated match $(x2, y2)$ inside the search area is computed. (c), (d) The procedure is repeated using the new position of the ROI $(x2, y2)$. (e), (f) Definition of variables for the time-domain correlation formula.

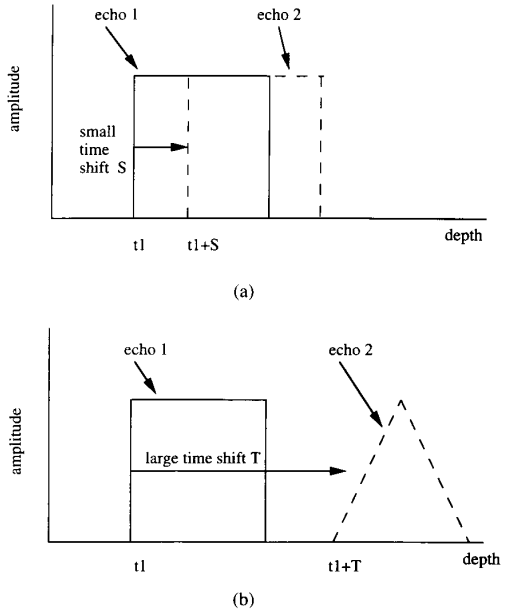

Fig. 2. Two ultrasonic echoes of a target before (echo 1) and after (echo 2) it has moved. (a) Echo 2 remains similar to echo 1 after the target has moved a small distance S. (b) For $T \gg S$, echo 2 looks decorrelated from echo 1 after the target has moved a large distance T.

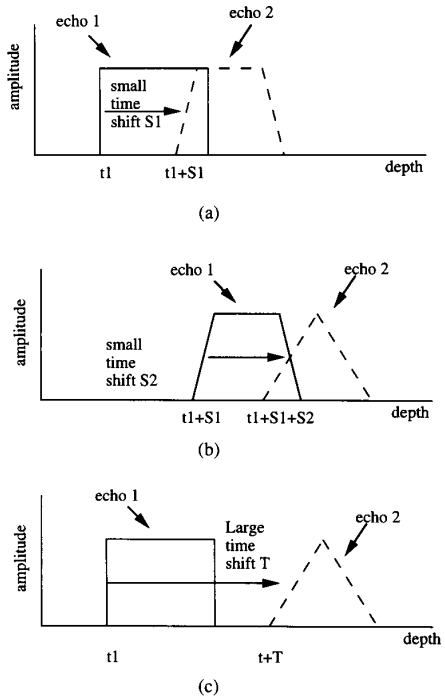

Fig. 3. Ultrasonic measurement of target motion using incremental tracking. (a), (b) Echo 2 remains similar to echo 1 after the target has moved a small distance $S1$ or $S2$. (c) Echo 2 looks decorrelated from echo 1 after the target has moved a large distance T. The movement can be estimated by incrementally tracking the target in smaller steps $S1, S2$ and then summing the steps $T = S1 + S2$.

search, the temporal shift between the initiation of two echoes can be used to estimate both displacement and velocity. Note that echo 2 remains similar to echo 1 after the target has moved a smalld distance. The problem with this method is that the ultrasonic speckle signature of a target changes with increasing target translations [3], [4]. In Fig. 2(b), this is represented schematically by a square pulse becoming a triangle. Echo 2 is not only temporally shifted from echo 1, but now also appears different from echo 1.

The problem can be reduced by tracking the target over shorter distances. This is done by computing the ROI's displacement between successive echoes. In Fig. 3(a) and (b), the target moves a small distance (on the order of a few wavelengths). As a result, the second echo becomes only slightly decorrelated from the first echo. This is shown schematically as a square pulse becoming a trapezoid and as a trapezoid becoming a triangle. The large target displacement [Fig. 3(c)] can be estimated by incrementally tracking the target displacement in smaller steps. By *incrementally* estimating the target's displacements and then summing the displacements, a good estimate of the target's *net* displacement can be obtained. It is important to note that incremental tracking can improve performance by reducing the component of speckle decorrelation that is due to target motion. It cannot compensate for the component of speckle decorrelation that is due to random noise generated by electrical and acoustical sources.

A user-defined search region can be employed to reduce both computational time and the number of computations. In this study, a search region extending out 1.0 cm from the target, in each dimension, was automatically selected. The increased accuracy achieved using the incremental tracking strategy was experimentally verified and documented in a previous study [1]. Fig. 4 (adapted from [1]) illustrates the improved performance of the incremental technique for tracking a 1.25 × 1.25 cm sponge target.

III. Ultrasonic Measurement of Tissue Displacement

Sections of porcine longissimus muscle and porcine liver were obtained from the Meat Science Laboratory, Department of Animal Sciences, at the University of Illinois. The porcine samples were obtained within 24 h of death, and were vacuum sealed. All measurements were made at room temperature (≈22°C). Samples of porcine liver, porcine muscle, and woolen sea sponge were placed in a water tank and secured on top of sound-absorbing slabs. Ultrasonic B-mode sector scans (video-detected signals) were obtained using a 5 MHz, 724A ATL servocontrolled rotary transducer coupled to an ATL MK 500 ultrasonic imaging system.

Each of the sample types was placed in contact with the imaging transducer, and was positioned in the center of the transducer's beam axis. Porcine liver and muscle samples were imaged in a manner that covered the entire field of view of the B scans. The physical dimensions of the porcine liver and muscle samples were many times larger (an order of magnitude) than the dimensions of the ROI's selected from the image.

To simulate axial displacements, the imaging transducer was translated along the beam axis using a high-precision Daedal

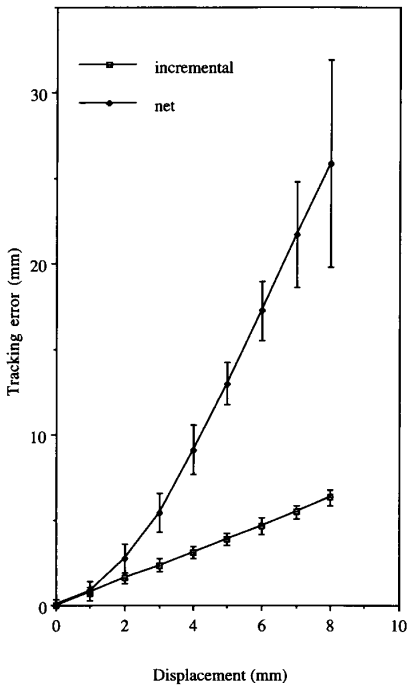

Fig. 4. Performance of the incremental tracking strategy in estimating axial displacement. Data points are the linearly weighted average of 10 minus d measurements for each data point, where d represents the axial displacement (in millimeters) of a sponge sample. Error bars represent two standard deviations. Lateral results show a similar trend.

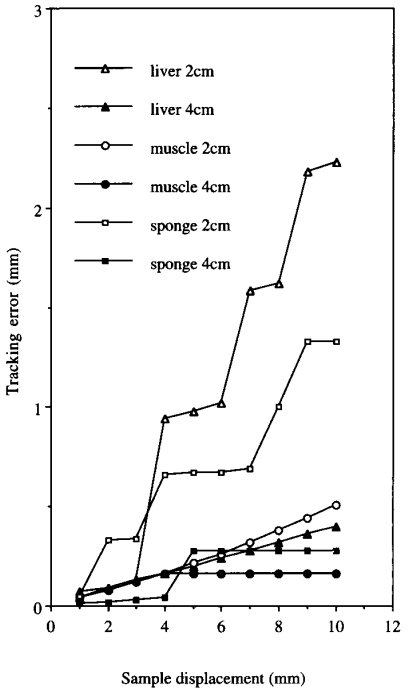

Fig. 5. Performance of the time-domain correlation technique for 6 of the 24 ROI's tested. The 6 ROI's were representative of the results from all 24 ROI's tested in the experiment. For identical target dimensions and displacements, ROI's in liver produced the largest tracking errors.

motorized positioning system (precision of 1 μm for axial and lateral motions). The positioning system is computer controlled and has 5 degrees of freedom, three translational and two rotational. Video-detected signals were digitized and saved using a Targa 16 frame-grabbing system and a Compaq 386 computer. Once all of the data were acquired, the data were transported to a Sun Sparc 2 workstation. 24 different ROI's were selected from individual samples of porcine liver, porcine muscle, and woolen sea sponge. The ROI's had dimensions ranging from 1.0 mm (approximately three times the axial resolution of the imaging system) to 5.0 cm (approximately 160 times the axial resolution of the imaging system). The time-domain correlation technique was implemented in C language code on a Sun Sparc 2 workstation and was used to estimate ROI displacements.

IV. Results

A. Accuracy of Ultrasonic Displacement Estimates as a Function of Scattering Media

Fig. 5 shows the tracking error in ultrasonic displacement estimates for 6 of the 24 ROI's selected from images of porcine liver and muscle samples and woolen sea sponge. The results from these ROI's were representative of the results from all 24 ROI's tested in the experiment.

For identical target dimensions and sample displacements, ultrasonic displacement estimates in muscle samples produced smaller errors than in liver samples. ROI's from the sponge showed errors between those found for ROI's in liver and muscle. Muscle tissue is composed of thousands of cylindrical muscle fibers, with diameters ranging from 10 to 100 μm and with lengths extending as long as 30 cm [10]–[13]. Inside the muscle fibers themselves are cylindrical elements (myofibrils) 1–2 μm in diameter. Myofibrils occupy approximately 80% of fiber volume.

The structured morphology of muscle tissue appears to provide more high spatial frequency information, which corresponds to more textural detail than liver tissue. This seems to improve the performance of the cross-correlation technique. This result is not surprising if we consider the fact that it should be easier to perform two-dimensional tracking in areas that contain distinct landmarks rather than in areas that are more uniform. The improvement in ultrasonic displacement estimates in porcine muscle samples can thus be partially attributed to the internal composition of porcine muscle, which contains well-defined fibers [10]–[13]. Liver tissue is predominantly composed of hepatic and kupfer cells. The cells are polyhedral in shape and have dimensions ranging from approximately 200 to 400 μm. Despite the presence of portal and hepatic veins, the internal composition of liver is mostly homogeneous [14]–[17]. It follows that the deterioration of ultrasonic displacement estimates in porcine liver may be a result of the more homogeneous composition of porcine liver compared to muscle tissue.

It has been established that the performance of ultrasonic displacement and velocity estimation algorithms generally improves with increasing signal-to-noise ratio (SNR) [4], [7], [8]. Because ultrasonic echoes result from internal tissue variations of acoustic properties, differences in the variation of propagation velocity inside porcine liver and porcine muscle may result in a higher SNR in echoes received from muscle compared to liver. The propagation velocities for the three sample types are all within 5% of one another; however, there may still be a nominal effect on displacement estimates.

Finally, it is known that the accuracy of ultrasonic displacement and velocity estimates generally improves with increasing frequency of interrogation [4], [5], [7]. Attenuation effects in liver and muscle tissue can result in a downshift of the center frequency of the spectrum of received echoes. Differences in the variation of acoustical properties inside porcine liver and porcine muscle tissues may result in different downshifts in the center frequency in echoes received from muscle compared to liver. The difference in attenuation between porcine liver and porcine muscle is relatively small (less than 10% [18]–[19]), and the downshift in frequency due to attenuation is usually small (on the order of a few hundred kilohertz in liver tissue for a center frequency of 5.0 MHz) so the contribution from these effects should remain relatively minor.

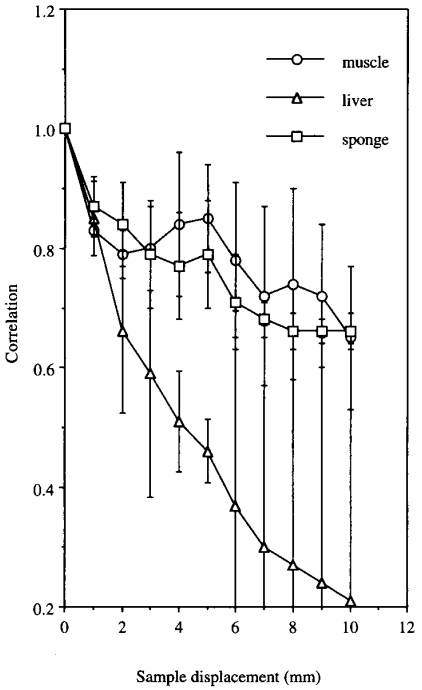

Fig. 6. Decorrelation of speckle patterns in liver, muscle, and woolen sea sponge samples with increasing sample displacements. Data points were averaged from five 4.0 cm ROI's for each sample type. Error bars represent one standard deviation.

B. Accuracy of Ultrasonic Displacement Estimates as a Function of Displacement

Fig. 6 provides a measure of how much the speckle patterns from each of the sample type change with distance. Because speckle-tracking algorithms rely on a minimal distortion in speckle patterns after target translations [4], displacement estimates are therefore accurate only to the extent that speckle patterns remain stable or do not change significantly with tissue translations. We observe that in the range of 0.0–3.0 mm, liver speckle patterns decorrelated more rapidly than muscle speckle patterns. This suggests that for a given displacement, and with all other factors held constant, ROI's in liver samples become less recognizable when compared to a reference signal than ROI's in muscle samples. As a result, it is not surprising that displacement estimates in muscle samples were found to be better than in liver samples.

For all 24 targets tested, the accuracy of ultrasonic displacement estimates deteriorated with increasing sample displacements. The increase in tracking errors for increasing sample displacements makes sense because all target speckle patterns decorrelated with increasing sample displacements.

The decorrelation of speckle patterns with increasing displacement are similar to those reported by Ramamurthy and Trahey [4] for liver-mimicking samples.

C. Accuracy of Ultrasonic Displacement Estimates as a Function of Target Dimensions

For all 24 targets tested, the accuracy of ultrasonic displacement estimates improved with increasing target dimensions. The improved performance of the cross-correlation technique for large target regions can be attributed to the large number of pixels or information present in large ROI's.

A useful conceptualization is that the ROI can be thought of as a missing person. Each pixel value in the ROI represents a characteristic used to describe the person such as height, weight, age, etc. Each possible target region in the search area can be thought of as a single person in a crowd of people. In this scenario, we are given a description or list of characteristics that describe the missing person (i.e., the pixel values in the ROI), and we are told that the missing person has walked into a crowd of people. The goal is to find the person in the crowd (search area) who "best fits" (correlates to) the description of the missing

As the number of pixels in the ROI (or descriptors of the missing person) increases, so does our confidence that the person in the crowd best matching the description is actually the missing person. In addition, as ROI dimensions increase, the number of possible target regions in a fixed size search area decreases. Conceptually, the number of people in the crowd decreases. This also contributes to the improved accuracy for large ROI's (dimensions large relative to the resolution of the imaging system). However, given a large number of pixels in the ROI (or descriptors), the person in the crowd (or target region in the serch area) best matching the description may not match all of the descriptors (low correlation coefficients, not an exact match) of the missing person.

As the number of pixels or descriptors decreases, the easier it becomes to find a person in the crowd who matches

most or all of the descriptors of the missing person (high correlation coefficient). However, with a smaller list of descriptors, the number of people in the crowd matching the description of the missing person now increases (number of false peaks increases, accuracy decreases as dimensions of ROI are reduced). In addition, as ROI dimensions decrease, the number of possible target regions in a fixed size search region increases, and this can also contribute to reduced accuracy for small ROI's.

From our experimental results, we note that large ROI's (ROI dimensions greater than ten times the axial resolution of the imaging system) generally tended to produce a low-amplitude correlation peak. The low amplitude of the correlation peak indicates difficulty in finding a target region in the search area providing an exact match to the ROI. For the case of large ROI's, the central lobe of the correlation peak as well defined with low-amplitude sidelobes. The clearly defined peak and low sidelobes indicate a high degree of confidence that the target region in the search area, best matching the ROI, does indeed correspond to the ROI.

Speckle tracking small ROI's (ROI dimensions on the order of the axial resolution of the imaging system) typically produced a high-amplitude (peak amplitude > 0.90) correlation peak with a large number of high-amplitude sidelobes. The high amplitude of the correlation peak indicates a good match between the corresponding pixel values in the ROI and the best correlated target region. Both the large number and high amplitude of the sidelobes indicate a low degree of confidence that the best correlated target region in the search area actually corresponds to the ROI. Smaller ROI's appear to be more susceptible to false matches. This is in agreement with the findings of Foster *et al.* [6] for one-dimensional signals and Chen *et al.* [1], [2] and Ramamurthy and Trahey [4] for two-dimensional signals.

The results of applying the cross-correlation speckle-tracking technique in tracking rectangular ROI's with axial dimensions of 75 times, 15 times, and 1.5 times the axial resolution of the imaging system are shown in Fig. 7(a)–(c), respectively. The axial resolution of the imaging system used was approximately 0.3 mm. ROI dimensions are thus provided in terms of the axial resolution.

The starting position of each target was the center of the rectangular grid. Each target was translated axially downward by 1.0 mm. A user-defined search region, which extended out by 1.0 cm in both dimensions, was centered on the starting position of each target. The contour plots represent the magnitude of the correlations at each position inside the search region. The horizontal and vertical axes represent a pixel coordinate system, where each pixel represents approximately 0.25 mm.

For the 5 cm target, the contour plot in Fig. 7(a) indicates a low-amplitude correlation peak that is well defined. For the 1 m target, Fig. 7(b) depicts a higher amplitude correlation peak. However, the correlation peak has been partially obscured by a number of secondary peaks that result from false matches. For the 1 mm target, the contour plot in Fig. 7(c) indicates that the location of the true correlation peak has now been completely obscure by a large number of high-amplitude false peaks.

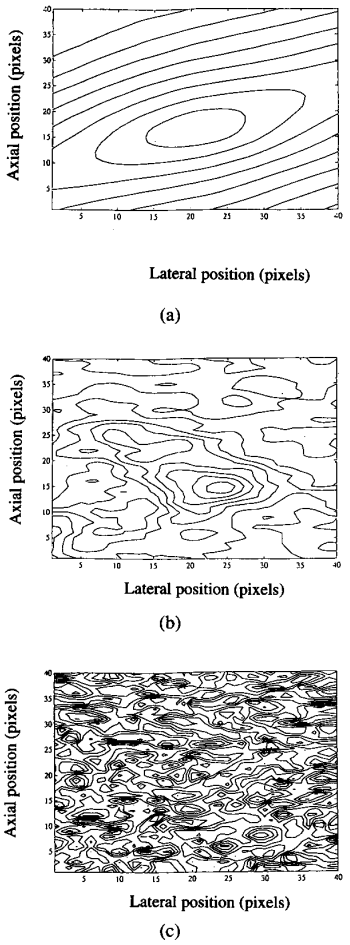

Fig. 7. Results from a typical frame-to-frame correlation search for 5×5 cm, 1×1 cm, and 1×1 mm targets selected from a sponge sample undergoing a 1.0 mm axial displacement. 1 pixel = 0.25 mm. (a) 5 cm target produces a low-amplitude correlation peak that is well defined. (b) For the 1 cm target, the position of the true correlation peak is partially obscured by secondary peaks that result from false matches. (c) For the 1 mm target, the plot is saturated by a large number of high-amplitude secondary "false" peaks. Position of true correlation peak is lost.

Fig. 7(a)–(c) illustrates that by selecting smaller target regions, the number of areas matching the target region increases. This produces an increasing number of ambiguous secondary correlation peaks until the position of the actual peak is lost. In this limiting case, the correlation search results are similar to an underdetermined system of equations where there is not a unique solution. Each correlation peak can be thought of as one possible solution to the system of equations which has not been given enough constraints (large enough target dimensions). The underdetermined system, therefore, does not have a unique solution because many different solutions (target regions) may satisfy the constraints (match the region of interest).

As target dimensions approach the resolution of the imaging system, the target becomes comparable to the dimension of individual speckle cells. At these dimensions, the speckle pat-

terns from separate targets become indistinguishable from one another. For most tissues with large speckle cells, the number of independent speckles contained in a target region may be reduced [5], and a large speckle cell size may contribute to less information being available per unit area for target regions. This is in agreement with the theory for object structures that are correlated [5].

D. Covariance Curves for Liver and Muscle Samples

The autocovariance functions for liver, muscle, and sponge samples were generated by correlating ROI's from each sample type with shifted versions of itself. Data points were averaged from covariances computed from ten images for each sample type.

For video-detected signals, a sharp and narrow sample covariance curve suggests that speckle tracking might produce sharp cross-correlation peaks with low sidelobes. This would reduce tracking errors due to false peaks and jitters as defined by Ramamurthy and Trahey [4]. A broad autocovariance curve suggests that speckle-tracking targets would result in correlation peaks consisting of a broad central lobe with higher sidelobes. This would increase tracking errors due to jitter and false peaks.

A narrow covariance curve also implies a small speckle cell size (using the full-width half-max FWHM definition [5]). In the lateral dimension, the speckle cell size is inversely proportional to the frequency of interrogation. Thus, for the same sample types and target dimensions, target regions will likely contain more independent speckles, and thus more information per unit area at higher frequencies.

Based on this discussion, we would expect porcine liver to produce the broadest autocovariance curve and porcine muscle to produce the narrowest autocovariance curve *if* differences in the speckle characteristics (and their first- and second-order statistics) for each tissue type are *actually* responsible for the improved accuracy observed when tracking ROI's in porcine muscle compared to porcine liver.

The *actual* covariance curves are, in fact, virtually identical (Fig. 8). This is not completely surprising since the propagation velocities (and wavelengths) for the three tissue types are within 5% of each other (liver = 1560 m/s, muscle = 1570 m/s, sponge = 1480 m/s), and the theoretical full-width at half-max (FWHM) point on the covariance curves predicted by Wagner *et al.* [5] is approximately 0.33 mm, close to the axial resolution of the imaging system.

The fact that the autocovariance curves for the three tissue types are virtually identical suggests that the improvement in displacement estimates in muscle samples *is not*, in fact, due to differences in the speckle characteristics and statistics between liver and muscle. The covariance curves do *not*, however, rule out the possibility that the improved displacement estimates in muscle may be attributed to the presence of well-defined and *resolvable* muscle fibers, whose lengths fall in the range of 2–30 cm [10]–[13], much larger than the axial resolution of the imaging system, and the complete *lack* of such resolvable internal structures in liver tissue which is largely homogeneous [14]–[17].

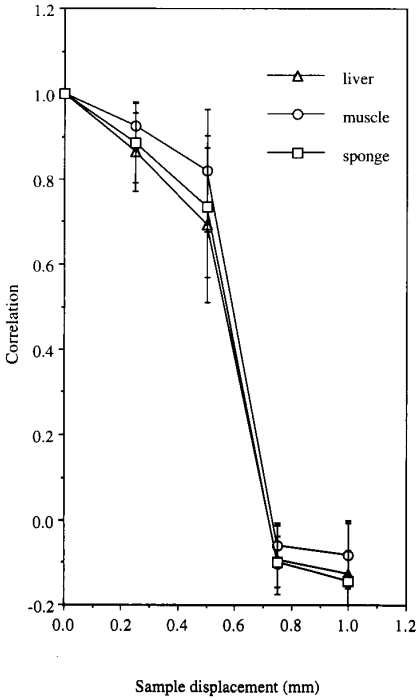

Fig. 8. Autocovariance curves for porcine liver, porcine muscle, and woolen sea sponge. Data points are the average of covariances computed from ten images for each sample type. Error bars represent two standard deviations.

E. Other Factors

We have primarily focused our attention on the influence of different tissue types on displacement and velocity estimation. However, the accuracy of ultrasonic displacement and velocity estimates depends on many factors, some of which have been studied by other investigators. We now review the impact of some of the other factors on displacement and velocity estimation that have been reported to date.

The accuracy of ultrasonic displacement and velocity estimates deteriorates for lateral sample displacements [4], [5]. This is attributed to the lower resolution achieved when imaging in the lateral direction. Higher ultrasonic frequencies of interrogation increase both axial and lateral resolution, and this results in improved accuracy in ultrasonic displacement estimates [2], [4]–[6].

The digital sampling frequency, or the rate at which the backscattered RF signal is digitized, determines the smallest steps or units of temporal shift in which signals may be correlated. Thus, while ultrasonic frequency of interrogation, tissue propagation speed, and transducer geometry establish the physical resolution limits of the imaging system, the digital sampling frequency similarly establishes the resolution limit for computational analysis. Parilla *et al.* [7] have reported reduced errors in ultrasonic range measurements in air with increasing digital sampling frequency. They also suggest that sampling above five times the ultrasonic frequency of interrogation should make the system signal-to-noise ratio the limiting factor.

TABLE I

Parameter	Impact
Displacement (Magnitude)	Backscattered signal decorrelates with increasing displacement, causing accuracy of ultrasonic displacement and velocity estimates to deteriorate with displacement.
Displacement (Direction)	Improved accuracy in axial dimension due to higher resolution in that dimension.
Target Dimensions	Accuracy improves with increasing target dimensions. Small target dimensions may result in an underdetermined system and false correlation peaks.
Scattering Media	Liver samples (homogeneous-type media) produced largest errors. Muscle samples (containing well-defined and highly resolvable fibers) had smallest errors.
Ultrasonic Frequency	Increasing ultrasonic frequency of interrogation increases accuracy due to improved axial and lateral
Digital Sampling Frequency	Higher digital sampling frequency results in smaller errors due to improved resolution in computational analysis. Sampling above five times the ultrasonic frequency of interrogation causes the system signal-to-noise ratio to be the limiting factor.
Signal Type	Higher accuracy is achieved in all cases by processing RF signals. Averaging and lower resolution reduce accuracy in envelope-detected signals.

Ultrasonic displacement and velocity measurements obtained from processing RF data will be substantially better than those obtained by processing envelope-detected signals. The RF data provide a larger number of data points, corresponding to a smaller unit of distance between points, which improves the resolution in computational analysis. Smaller details in the RF signal may also be averaged out in the detection process, and may not appear in the envelope signal. These results have been predicted by Wagner *et al.* [5], and experimentally verified by Ramamurthy and Trahey

F. Summary of Imaging Factors Impacting Ultrasonic Displacement and Velocity Estimation

Table I is a summary of the impact of various imaging parameters on ultrasonic displacement and velocity estimates. This is based on the results reported by Chen *et al.* [1]–[3], Ramamurthy and Trahey [4], Wagner *et al.* [5], Foster *et al.* [6], Parilla *et al.* [7], Ferrara [8], and Bonnefous and Pesque [9].

V. Conclusion

The impact of important imaging parameters on ultrasonic displacement and velocity measurements has been discussed. The impact of different scattering media, which has not received significant attention in the past, has been explored with experimental results and computer analysis. The accuracy of ultrasonic displacement estimates was found to be better in porcine muscle samples than in porcine liver samples. Analysis of experimentally derived autocovariance curves for each tissue type indicates that the improvement in accuracy for muscle samples *was not*, in fact, due to differences in the speckle characteristics for each tissue type. The improvement was attributed to the presence of well-defined and *resolvable* image structures (possibly from muscle fibers) and the lack of such resolvable internal structures in porcine liver tissue. In addition to tissue morphology, differences in tissue reflectivity, which may affect SNR, and tissue attenuation, which can shift center frequency, may also contribute significantly to the influence of different tissue types on ultrasonic displacement and velocity estimation.

Although we have focused attention on the influence of different tissue types, the accuracy of ultrasonic displacement and velocity estimates depends on many factors. Many of these have been studied, and a compilation of results from our work and those of other investigators has shown several fundamental results.

The accuracy of ultrasonic displacement and velocity estimates improves with increasing target dimensions, ultrasonic frequency of interrogation, and digital sampling frequency. Performance deteriorates for increasing displacements. There is a significant improvement in all estimates for measurements taken in the axial direction, and for ultrasonic displacement and velocity estimates obtained by processing RF data instead of envelope-detected data.

References

[1] E. J. Chen, W. K. Jenkins, and W. D. O'Brien, Jr., "Accuracy and precision of estimating tissue displacements from ultrasonic images," presented at the IEEE Ultrason. Symp., 1992.
[2] E. J. Chen, "Uncertainty in estimating tissue motion from ultrasonic images," M.S. thesis, Univ. Illinois, Urbana, May 1992.
[3] E. J. Chen, I. A. Hein, R. S. Adler, P. L. Carson, and W. D. O'Brien, Jr., "A comparison of the motion tracking of ultrasonic B-mode tissue images with a calibrated phantom," in *Proc. IEEE Ultrason. Symp.*, 1991, vol. 2, pp. 1211–1214.
[4] B. S. Ramamurthy and G. E. Trahey, "Potential and limitations of angle-independent flow detection algorithms using radio frequency and detected echo signals," *Ultrason. Imaging*, vol. 13, pp. 252–268, 1991.
[5] R. Wagner, S. Smith, J. Sandrik, and H. Lopez, "Statistics of speckle in ultrasonic B-scans," *IEEE Trans. Son. Ultrason.*, vol. SU-30, no. 3, pp. 156–163, 1985.
[6] S. Foster, P. Embree, and W. D. O'Brien, Jr., "Flow velocity profile via time-domain correlation: Error analysis and computer simulation," *IEEE Trans. Ultrason. Ferroelec., Freq. Contr.*, vol. 37, no. 2, pp. 164–175, 1990.
[7] M. Parilla, J. J. Anaya, and C. Fritsch, "Digital signal processing techniques for high accuracy ultrasonic range measurements," *IEEE Trans. Instrum. Meas.*, vol. 40, no. 4, pp. 759–763, 1991.
[8] K. Ferrara, "Comparison of estimation strategies for determination of blood velocity using ultrasound," *Acoust. Imaging*, vol. 18, pp. 327–337, 1991.
[9] O. Bonnefous and P. Pesque, "Time domain formulation of pulse-Doppler ultrasound and blood velocity estimation by cross-correlation," *Ultrason. Imaging*, vol. 8, pp. 73–85, 1986.
[10] B. Hete and K. Shung, "Scattering of ultrasound from skeletal muscle tissue," *IEEE Trans. Ultrason. Ferroelec., Freq. Contr.*, vol. 40, pp. 354–365, July 1993.
[11] R. M. Berne and M. N. Levy, *Principles of Physiology*. St. Louis, MO: Mosby, 1990.

[12] A. J. Varder, J. H. Sherman, and D. S. Luciano, *Human Physiology*. New York: McGraw-Hill, 1985.
[13] B. Alberts, D. Bray, J. Lewis, M. Raff, K. Roberts and J. Watson, *Molecular Biology of the Cell*. New York, London: Garland, 1989.
[14] H. Popper and F. Schaffner, *Liver Structure and Function*. New York: McGraw-Hill, 1957.
[15] T. Hargreaves, *The Liver and Bile Metabolism*. Meredith Corporation, 1968.
[16] W. H. Andrews, *Liver*. Edward Arnold, 1979.
[17] H. Elias and J. Sherrick., *Morphology of the Liver*. New York: Academic, 1969.
[18] S. A. Goss, R. L. Johnston, and F. Dunn, "Comprehensive compilation of empirical ultrasonic properties of mammalian tissues," *J. Acoust. Soc. Amer.*, vol. 64, Aug. 1978.
[19] ——"Comprehensive compilation of empirical ultrasonic properties of mammalian tissues II," *J. Acoust. Soc. Amer.*, vol. 68, July 1980.

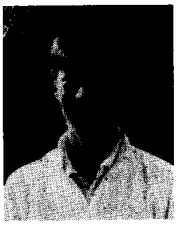

Eric J. Chen received the B.S. and M.S. degrees in electrical and computer engineering from the University of Illinois in 1990 and 1992, respectively.

In 1991 he received a National Institutes of Health Radiation Oncology Trainee Fellowship. In the summer of 1993 he worked in the Biomedical Sciences Division at Lawrence Livermore National Laboratory, where he developed image analysis and visualization software for computer-aided screening of high-resolution digital mammograms. He is currently a member of the Bioacoustics Research Lab at the University of Illinois, where he has done extensive work developing systems for nondestructive imaging of soft tissue elasticity and 2-D imaging of tissue motion using ultrasound. From 1990 to 1992 he was also a Network and Computer Systems Administrator at the Coordinated Sciences Research Laboratory at the University of Illinois. He is also currently working towards the Ph.D. degree at the University of Illinois.

W. Kenneth Jenkins (F'85) received the B.S.E.E. degree from Lehigh University, Bethlehem, PA, in 1969 and the M.S.E.E. and Ph.D. degrees from Purdue University, West Lafayette, IN, in 1971 and 1974, respectively.

From 1974 to 1977, he was a Research Scientist Associate in the Communications Sciences Laboratory at the Lockheed Research Laboratory, Palo Alto, CA. In 1977, he joined the faculty at the University of Illinois at Urbana-Champaign, where he is currently a Professor with the Electrical and Computer Engineering Department and the Coordinated Sciences Laboratory. Since May 1987, he has been Director of the Coordinated Sciences Laboratory and Principal Investigator on the Joint Services Electronics Program (JSEP) at the University of Illinois. His current interests include digital filtering, signal processing algorithms, multidimensional array processing, computer imaging, one- and two-dimensional adaptive digital filtering, and VLSI architectures for signal processing.

Dr. Jenkins is a past Associate Editor for the IEEE TRANSACTIONS OF CIRCUITS AND SYSTEMS, and has served as the Sectretary-Treasurer (1982–1983), President-Elect (1984), and President (1985) of the CAS Society. Also, he has served as General Chairman of the 32nd Midwest Symposium on Circuts and Systems (1988) and the Program Chairman of the 1990 IEEE International Symposium on Ciruits and Systems. He is a member of Phi Eta Sigma, Eta Kappa Nu, and Tau Beta Pi. He was the recipient of the 1977 Lockheed Publication Award, and in 1978 was awared the first Myril B. Reed Best Paper Award at the International Conference on Circuits an Computers for the best technical presentation in Alogorithms and Architectures. Also in 1985, he was elected Fellow of the IEEE for his professional contributions in digital signal processing and engineering education. In 1990, he was awarded the Distinguished Service Award of the IEEE Circuits and Systems Society for important and sustained professional contributions to the Society over many years.

William D. O'Brien, Jr.(S'64–M'70–SM'79–F'89) was born in Chicago, IL, on July 19, 1942. He received the B.S., M.S., and Ph.D. degrees in 1966, 1968, and 1970 from the University of Illinois, Urbana-Champaign.

From 1971 to 1975, he worked with the Bureau of Radiological Health (currently the Center for Devices and Radiological Health) of the U.S. Food and Drug Administration. Since 1975 he has been with the University of Illinois, where he is a Professor of Electrical and Computer Engineering and of Bioengineering, College of Engineering, and Professor of Bioengineering, College of Medicine and is the Program Director of the Radiation Biophysics and Bioengineering in Oncology Training Program. His research interests involve the many areas of ultrasound-tissue interaction, including spectroscopy, risk assessment, biological effects, tissue characterization, dosimetry, blood-flow measurements, acoustic microscopy, and meat characterization for which he has published more than 110 papers.

Dr. O'Brien is Editor-in-Chif of the IEEE TRANSACTIONS ON ULTRASONICS, FERROELECTRICS, AND FREQUENCY CONTROL. He is a Fellow of the Acoustical Society of America and the American Institute of Ultrasound in Medicine (AIUM) and was recipient of an IEEE Centennial Medal (1984), the AIUM Presidential Recognition Award (1985), the AIUM/WFUMB Pioneer Award, and the IEEE Outstanding Student Branch Counselor Award (1989). He was a recently inaugurated as a Founding Fellow of American Institute of Medical and Biological Engineering. He was President (1982–1983) of the IEEE Sonics and Ultrasonics Group (currently the IEEE UFFC-Society), Co-Chairman of the 1981 IEEE Ultrasonics Symposium and General Chairman of the 1988 IEEE Untrasonics Symposium. He was also the President of the AIUM (1988–1991) and is currently the Treasurer of the World Federation for Ultrasound in Medicine and Biology.